Association of double tropopause events with baroclinic waves

J. M. Castanheira[1] and L. Gimeno[2]

Received 27 April 2011; revised 8 July 2011; accepted 16 July 2011; published 12 October 2011.

[1] We herein propose a method for identifying breaks in the subtropical tropopause as found in the ERA Interim reanalysis data. The method uses the identification of double tropopauses and allows the quantification of the extension of the overlap between the tropical and extratropical tropopauses. The correlations between the meridional extension of the superposition of tropopauses and the fields of geopotential, potential vorticity, or potential temperature, reveal baroclinic wave patterns. Similar wave patterns were also identified in the potential temperature fields derived from GPS radio occultation COSMIC data. The zonal propagation velocity of the anomalies in the meridional extension of the overlap was estimated using Hovmöller diagrams. The estimated zonal velocities suggest that the variability in the superposition of the tropopauses is associated with baroclinic Rossby wave patterns in the subtropical upper troposphere and lower stratosphere.

Citation: Castanheira, J. M., and L. Gimeno (2011), Association of double tropopause events with baroclinic waves, *J. Geophys. Res.*, *116*, D19113, doi:10.1029/2011JD016163.

1. Introduction

[2] Over the past decade, the study of the tropopause has been of increasing interest because its characteristics are important for understanding the exchanges between the troposphere and the stratosphere and may provide some important evidence associated with climate change [e.g., *Santer et al.*, 2003; *Seidel and Randel*, 2007; *Pan et al.*, 2009; *Birner*, 2010; *Gettelman et al*, 2010]. One of the phenomena that have been investigated recently is the occurrence of double tropopauses (DTs) [*Schmidt et al.*, 2006; *Randel et al.*, 2007; *Añel et al.*, 2008]. Such studies have used data from radiosondes, reanalyses and GPS radio occultation profiles, and have consistently shown that DT events occur much more frequently in the subtropical regions of both Hemispheres than they do elsewhere.

[3] *Randel et al.* [2007] and *Pan et al.* [2009] suggested that the mechanisms responsible for the formation of double tropopause structures may include contributions from a thermally direct secondary circulation around the subtropical jet, which is associated with developing baroclinic waves and is accompanied by an excursion of the tropical tropopause over the extratropical one. *Castanheira et al.* [2009] suggested that DT events must be associated with baroclinic waves in the subtropical upper troposphere/lower stratosphere (UTLS). Such an association would explain the significant positive trends in the frequency of DT events identified in radiosonde data, concurrent with significant positive trends in the energy of baroclinic waves as seen in reanalysis data. *Wang and Polvani* [2011] studied the link between double tropopauses and midlatitude baroclinic eddies using a set of experiments on idealized life cycles. Their results showed that, if an extratropical tropopause inversion layer (TIL) is present in the balanced initial temperature profile, DTs occur spontaneously during the nonlinear stage of the life cycle of the baroclinic eddies.

[4] Despite the foregoing advances, no direct association between baroclinic waves and DT events has yet been found in any of the observed data. We herein aim to show a clear association between the alternation of single tropopause (ST) and DT events and baroclinic wave patterns through the use of reanalysis and GPS radio occultation data. The remaining of the paper is structured as follows: section 2 describes the data and the methodology, section 3 presents and discusses the results, and the final remarks in section 4 conclude the paper.

2. Data and Method

[5] The present study is based on the NH winter (DJF) ERA Interim reanalysis [*Dee et al.*, 2011] on isobaric levels at 00 and 12 UT, for the period 1989–2010, and on the GPS radio occultation profiles of temperature, pressure and humidity derived from the Constellation Observing System for Meteorology, Ionosphere and Climate (COSMIC) mission [*Anthes et al.*, 2008]. The ERA Interim reanalyses of the temperature, geopotential and Ertel potential vorticity (PV) fields were downloaded from the ECMWF Data Server, and GPS data were freely available from the University Corporation for Atmospheric Research (UCAR)/COSMIC program (at www.cosmic.ucar.edu/). The COSMIC data were available from mid April 2006 to the end of 2010, and we analyzed the four complete winters of 2006/07 to 2009/10. In general, more than 1500 daily COSMIC profiles were available, with a vertical resolution of 100 m from the surface to an altitude of ~40 km. The GPS data were already assimilated in the ERA-Interim data. However, the GPS profiles provide a much

[1]Department of Physics, CESAM, University of Aveiro, Aveiro, Portugal.
[2]EPhysLab, Faculty of Sciences of Ourense, University of Vigo, Ourense, Spain.

0148-0227/11/2011JD016163

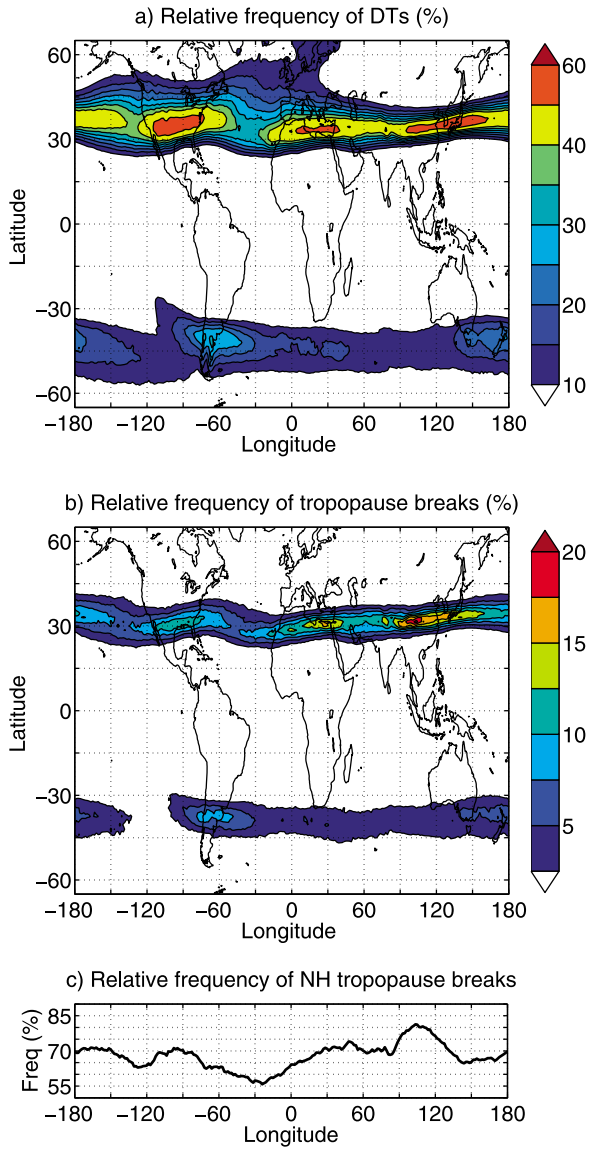

Figure 1. Relative frequencies of (a) double tropopause events and (b) tropopause breaks for the NH winter (DJF) season from the ERA Interim data. (c) The relative frequency of breaks in the NH tropopause as a function of the longitude, i.e., the sum of the relative frequencies of tropopausal breaks at each longitude in the NH.

greater vertical resolution than the reanalysis, and the vertical resolution of the data may influence the results based on diagnostics of the thermal lapse rate tropopause.

[6] The first and, if present, the second thermal lapse rate tropopauses were identified using the conventional WMO criterion:

[7] (a) The *first tropopause* is defined as the lowest level at which the lapse rate decreases to 2 K km^{-1} or less, provided also that the average lapse rate between this level and all higher levels within 2 km does not exceed 2 K km^{-1}.

[8] (b) If above the first tropopause the average lapse rate between any level and all higher levels within 1 km exceeds 3 K km^{-1} then a *second tropopause* is defined by the same criterion as in (a). This tropopause may be either within or above the 1 km layer.

[9] Because of the low (~1 km) vertical resolution in the UTLS, condition b) in the above definition was reduced to 2.5 K km^{-1} when analyzing the ERA Interim data. A similar procedure was applied by *Randel et al.* [2007], who reduced condition b) to 2 K km^{-1} in their analysis of the ERA40 data. The criteria used to find the tropopauses were applied using an algorithm that is similar to that used by *Birner* [2010] (which in turn is a slight variation of the algorithm used by *Reichler et al.* [2003]).

[10] As pointed out by *Randel et al.* [2007] and *Pan et al.* [2009], DTs are associated with characteristic breaks in the thermal tropopause near the subtropical jet, where the tropical tropopause extends to higher latitudes, overlying the lower extratropical tropopause. We herein identify the breaks in the thermal tropopause and measure the meridional extension of the superposition of tropopauses using the following rules, as applied to the ERA Interim reanalysis data:

[11] (a) For each longitude, we searched for double tropopause profiles, starting within the tropics (15°) and running polewards. The latitude of the break in the tropopause was the first latitude ϕ_b to have a double tropopause and which satisfied two further conditions. The first tropopause in the 15° band on the equatorward side of ϕ_b must have tropical characteristics ($150 \geq p_t \geq 70$ hPa, where p_t designates the tropopause pressure), and the first tropopause in the 15° band on the poleward side of ϕ_b must have extratropical characteristics ($160 \leq p_t \leq 400$ hPa).

[12] (b) For each longitude, we carried out a further search for double tropopause profiles, beginning at a high latitude (60°) and running equatorwards. If a break ϕ_b was found in a), it follows that when running equatorwards, a latitude ϕ_p with a double tropopause and $|\phi_p| \geq |\phi_b|$ must be found, corresponding to the poleward extension of the overlap of the tropical tropopause with the extratropical one. The first or second tropopause in the 15° band on the equatorward side of ϕ_p must have tropical characteristics ($150 \geq p_t \geq 70$ hPa), and the first tropopause in the 15° band on the poleward side of ϕ_p must have extratropical characteristics ($160 \leq p_t \leq 400$ hPa).

[13] The absolute difference $\Delta\phi = |\phi_p - \phi_b|$ is the latitudinal width of the superposition of the tropopauses.

[14] Figures 1 and 2 illustrate the NH winter climatology of the breaks in the tropopause and show the reliability of the method applied to the ERA Interim data. Figure 1 shows the relative frequencies of DTs and of breaks in the tropopause, which were calculated at each grid point dividing respectively the numbers of DTs and breaks by the total number of reanalysis times (3790). As expected, the breaks occur in two zonal bands in the subtropical regions, with maxima of frequency near the maxima of the frequency of DTs (compare Figures 1a and 1b). Figure 1c shows the relative frequency of breaks in the NH tropopause as a function of longitude, i.e., the sum of the relative frequencies of tropopausal breaks at each longitude in the NH. The zonal mean frequency of tropopausal breaks is 68%, with a minimum of 56% in the central Northern Atlantic. One may conclude that, during the NH winter, a tropopausal break is occurring at each longitude around 68% of the time. Hence the occurrence of a tropopausal break (and DTs) at each longitude is in fact the rule, not the exception. Figure 2a shows NH winter (DJF) climatology of the zonal means of the zonal wind and pressure of the first lapse rate tropopause (LRT1). Figure 2b is similar to Figure 2a, but the time and zonal means were cal-

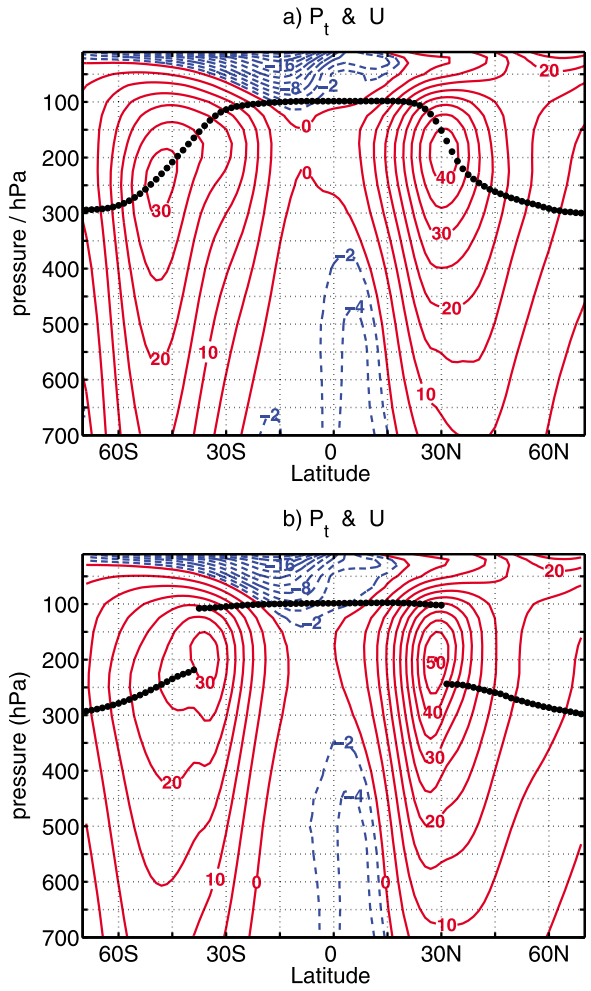

Figure 2. (a) NH winter (DJF) climatology of the zonal means of the zonal wind and pressure of the first lapse rate tropopause (LRT1) from the ERA Interim data. (b) Same as Figure 2a, but the time and zonal means were calculated including only those cases for which breaks in the tropopause were found. In Figure 2b the means of the zonal wind and the LRT1 pressure, in each hemisphere, were calculated as a function of the latitudinal distance to the latitude of the respective break. See the text for more details.

culated by including only those cases where breaks in the tropopause were found. Moreover, in Figure 2b, the zonal wind and the LRT1 pressure in each hemisphere were averaged as a function of the latitudinal distance to the latitude of the respective break, ϕ_b. The means were then plotted with respect to the mean latitude of the break, i.e., in Figure 2b, the latitudes in each hemisphere represent the mean position of the breaks plus the latitudinal distances. For example, considering the mean position of the break in the Northern Hemisphere at 31.5°N, the contours at latitude 15°N represent the means of the zonal winds found 16.5° equatorward of the instantaneous positions of the breaks. It may be seen that the breaks occur on the poleward side of the subtropical jet. The maxima of the zonal wind in Figure 2b are stronger and are shifted equatorwards in relation to the climatological mean. These characteristics are in accordance with the frequency distribution of the breaks (Figure 1b), whose maxima occur along the lines of the subtropical jet streams. A close comparison of Figure 1b with the NH winter climatology of the 200 hPa geopotential height field (not shown) reveals that the maxima in the frequency of tropopause breaks occur at the jet entrances, i.e., at the zones of confluence of the geopotential lines, where a thermally direct secondary circulation must exist to provide the Coriolis force necessary for the acceleration of the air particles. As suggested by *Randel et al.* [2007] and *Pan et al.* [2009] such a thermally direct secondary circulation may be involved in the mechanisms responsible for the formation of double tropopauses. The more frequent occurrence of tropopause breaks in the jet entrances may help to explain the positions of the maxima in the frequency of double tropopause events.

[15] All the correlation and regression analyses to be presented in the following section are based on climatological anomalies, i.e., all variables have had their seasonal cycles removed.

3. Results

3.1. Reanalysis

[16] Because of the low density of breaks in the tropopause in the SH during DJF (Figure 1b), only the breaks in the NH are analyzed herein. Figure 3 shows the zonal distributions of the standard deviations of, and correlations between ϕ_b, ϕ_p and $\Delta\phi$. The poleward extensions of the overlaps, ϕ_p, are more variable than the latitude of the breaks, ϕ_b (Figure 3a), and both show maxima and minima respectively on the eastern and western sides of the ocean basins. The correlation curves (Figure 3b) show that there are significant coherent meridional shifts in the limits of the overlaps of the tropopauses. The zonal mean of their correlation is $\bar{r}(\phi_b, \phi_p) = 0.52$. Moreover, a larger fraction of the variability of the meridional width, $\Delta\phi$, of the overlaps of the tropopause is due to their poleward extension. The zonal mean correlations of the meridional width, $\Delta\phi$, of the overlaps of the tropopause with their limits ϕ_b and ϕ_p are $\bar{r}(\Delta\phi, \phi_b) = -0.20$ and $\bar{r}(\Delta\phi, \phi_p) = 0.73$, respectively. Together, these statistics show that the variability of the overlaps of the tropopause results mainly from poleward excursions of the tropical tropopause and, to a much lesser degree, from equatorward displacements of the extratropical tropopause.

[17] The anomalies in the width of the overlap, $\Delta\phi$, have short time scales, with the autocorrelation function decreasing to zero in ~5 days. For such time scales, the tropopause variability must be due to dynamical rather than to radiative processes. The meridional displacements of ϕ_p relatively to ϕ_b must then occur in the presence of baroclinic motions. We hypothesize that such motions may be associated with baroclinic waves and, if this is the case, the increase and decrease in the extension of the overlaps of the tropopause are associated with wave anomalies of opposing sign. In order to test this hypothesis, we defined two regional indices of the meridional extensions of the overlaps of the tropopause over the western and eastern Pacific, where the variability of the extension of the overlap is at a minimum and a maximum, respectively. More specifically, we calculated one mean meridional width $\overline{\Delta\phi_{WP}}$ for the overlaps occurring in the longitudinal sector [127.5–141°E],

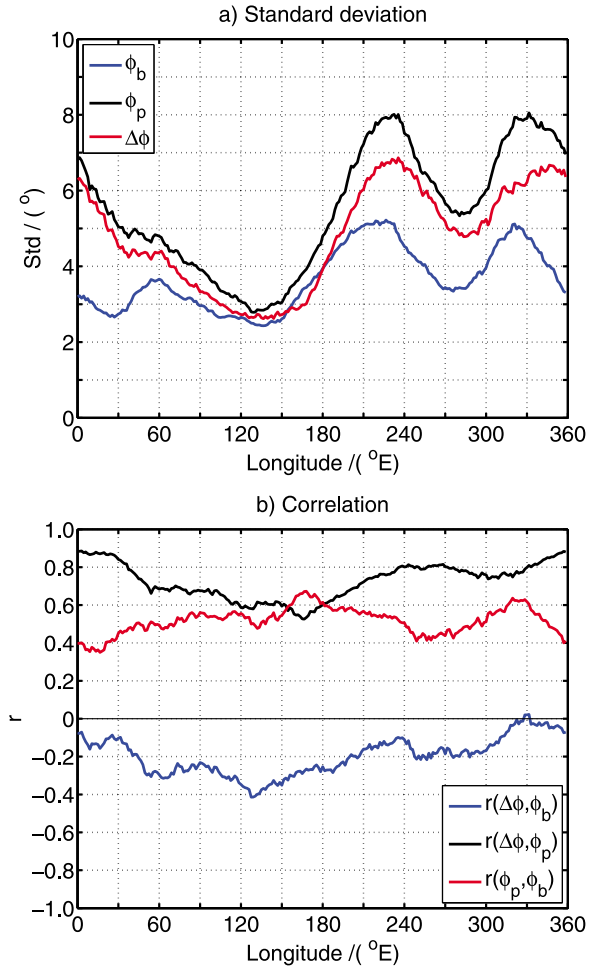

Figure 3. Zonal distributions of the (a) standard deviations of and (b) correlations between ϕ_b, ϕ_p and $\Delta\phi$ (see the text for the definition of these variables).

and another mean meridional width $\overline{\Delta\phi_{EP}}$ for the overlaps occurring in the longitudinal sector [225–238.5°E]. The frequencies of occurrence of tropopausal breaks at least at one grid longitude in the WP sector and at least at one grid longitude in the EP sector are 97% and 94%, respectively; so the indices were calculated for almost all times. We then obtained linear regressions of the PV and geopotential height fields on the indices $\overline{\Delta\phi_{WP}}$ and $\overline{\Delta\phi_{EP}}$. The linear regressions were performed onto these two indices to show that the characteristics associated with the variability of the overlap of the tropopauses are robust between the different regions. We repeated the calculations requiring different minimum numbers of tropopausal overlaps occurring in each longitudinal sector at each time. The results obtained remained qualitatively the same, even in the case we required that tropopausal overlaps occur at all grid longitudes in the sectors used to define $\overline{\Delta\phi_{WP}}$ and $\overline{\Delta\phi_{EP}}$.

[18] Figure 4 shows the maps of regression of PV and geopotential height at the 100 hPa level (PV_{100} and Z_{100}), which is the level closest to the mean pressure of the tropical tropopause and to the second lapse rate tropopause (LRT2). It may be seen that an increase in the overlap is associated with statistically significant local negative anomalies in PV and positive anomalies in geopotential. Moreover, the local anomalies are parts of wave patterns, which are more evident for the geopotential height field. The regression maps were obtained using daily values; i.e., before calculating the regressions, daily time series of each variable were obtained by averaging the respective values at 00 and 12 UT.

[19] Figure 5 shows the latitude-altitude correlation maps of the PV and potential temperature, θ, fields with $\overline{\Delta\phi_{WP}}$ and $\overline{\Delta\phi_{EP}}$. For each latitude and isobaric level we computed the mean of each variable in the longitudinal sectors [127.5–141°E] and [225–238.5°E], then computed the temporal correlation with the $\overline{\Delta\phi_{WP}}$ and $\overline{\Delta\phi_{EP}}$ time series, respectively. The correlation patterns were also calculated using daily values, and the vertical scale for their representation is the log-baric height $z = -7 \ln (p/p_0)$, where $p_0 = 1000$ hPa and z is given in km. Using the values in Figure 2, the mean heights of the extratropical LRT1 and tropical LRT1 near the NH break are ~10 km and ~16 km, respectively. The dipoles in the correlation maps for the PV may be seen to have a negative center around the level of the tropical tropopause and a positive center around the level of the extratropical tropopause. Since the PV has a sharp gradient across the extratropical tropopause and a strong poleward gradient in the subtropics [e.g., *Vallis*, 2007, Figure 12.21], the negative center can be associated with poleward excursions of the tropical tropopause, while the positive center can be associated with equatorward excursions of the extratropical tropopause. Because the tropical tropopause is higher than the extratropical ones, those motions would respectively replace stratospheric air by tropospheric air and tropospheric air by stratospheric air, thereby leading to the observed patterns of anomalies. The correlation patterns of the potential temperature are approximately in quadrature with the PV correlation patterns along the vertical. Such behavior may be expected because the PV is proportional to $\partial\theta/\partial p$, and the maxima and minima of the PV anomalies tend to be centered at the node lines of the potential temperature anomalies. Although the correlations outside the region of the break are small, they are nevertheless significant and suggest baroclinic wave structures. Here, and throughout the rest of the paper we use the term "baroclinic wave structures" do describe wave structures that change sign in the vertical. They need not necessarily have baroclinic instability as their source.

[20] The latitude-altitude cross sections of Figures 5a and 5b clearly indicate the motions of the tropopauses that are associated with the variability of their overlap. However, these patterns may miss some characteristics of the wave structures if there are zonal phase shifts with latitude and altitude. Figure 6 shows the regression patterns for the geopotential height fields at 10 and 300 hPa. By comparing regression patterns of Z_{300} (Figures 6c and 6d) with the regression patterns of Z_{100} (Figures 4c and 4d), it is possible to observe that the wave pattern across North America exhibits a westward phase tilt with height. Over the western Pacific, the positive regression center of Z_{100} on $\overline{\Delta\phi_{WP}}$ also shows a clear westward extension over a small negative center of the regression of Z_{300} onto $\overline{\Delta\phi_{WP}}$. The regression patterns of the Z_{10} are confined to higher latitudes and represent anomalies of small wavenumbers. Although a direct connection between the anomaly centers at 10 and

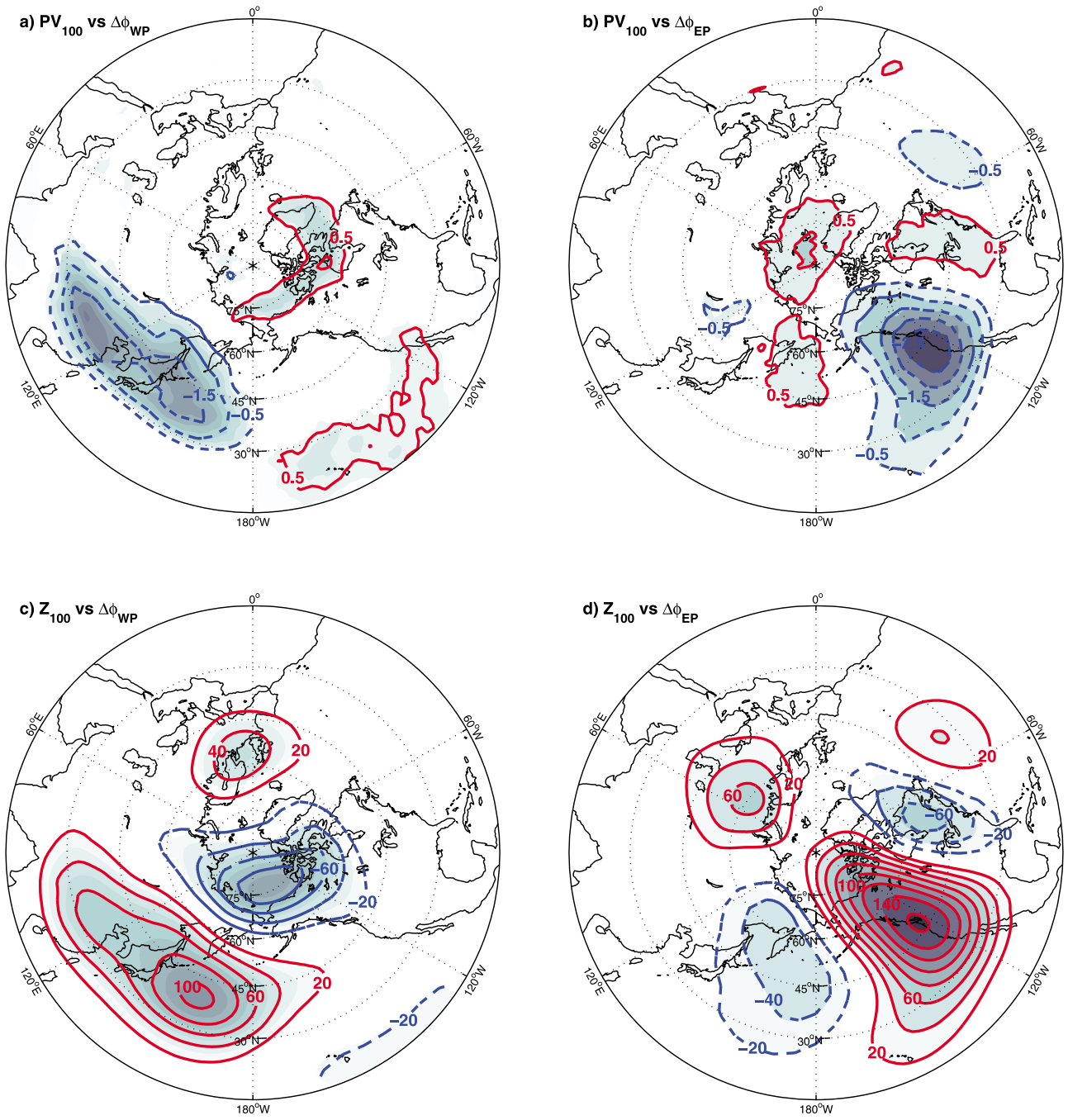

Figure 4. Regression patterns of the fields of 100 hPa potential vorticity (PV) and geopotential height, Z, on (a and c) $\overline{\Delta\phi_{WP}}$ and (b and d) $\overline{\Delta\phi_{EP}}$. The regression patterns represent the anomalies associated with 1.5 stdv of $\overline{\Delta\phi_{WP}}$ and $\overline{\Delta\phi_{EP}}$. Contour intervals are 0.5 PVU in Figures 4a and 4b and 20 gpm in Figures 4c and 4d. The zero contour is not shown. Shaded plots represent regression coefficients which are statistically significant at the 99% level.

100 hPa cannot be established, it is evident that the patterns at 10 hPa are rotated zonally with respect to the longitude of the anomalies seen at 100 hPa. For example, the wave patterns in Figures 4d and 6b appear in opposite hemispheres, with the anomalies in Figure 6b occurring at longitudes far from those where $\overline{\Delta\phi_{EP}}$ was defined (225–238.5°E). Moreover, the apparent planetary scale (wavenumbers 1 and 2) of the anomalies of Z_{10} suggests that the variability of the overlap of the tropopauses is associated not only with synoptic baroclinic eddies, but also with the excitation of planetary waves. The upward propagation of planetary waves requires that they have a westward phase tilt with height.

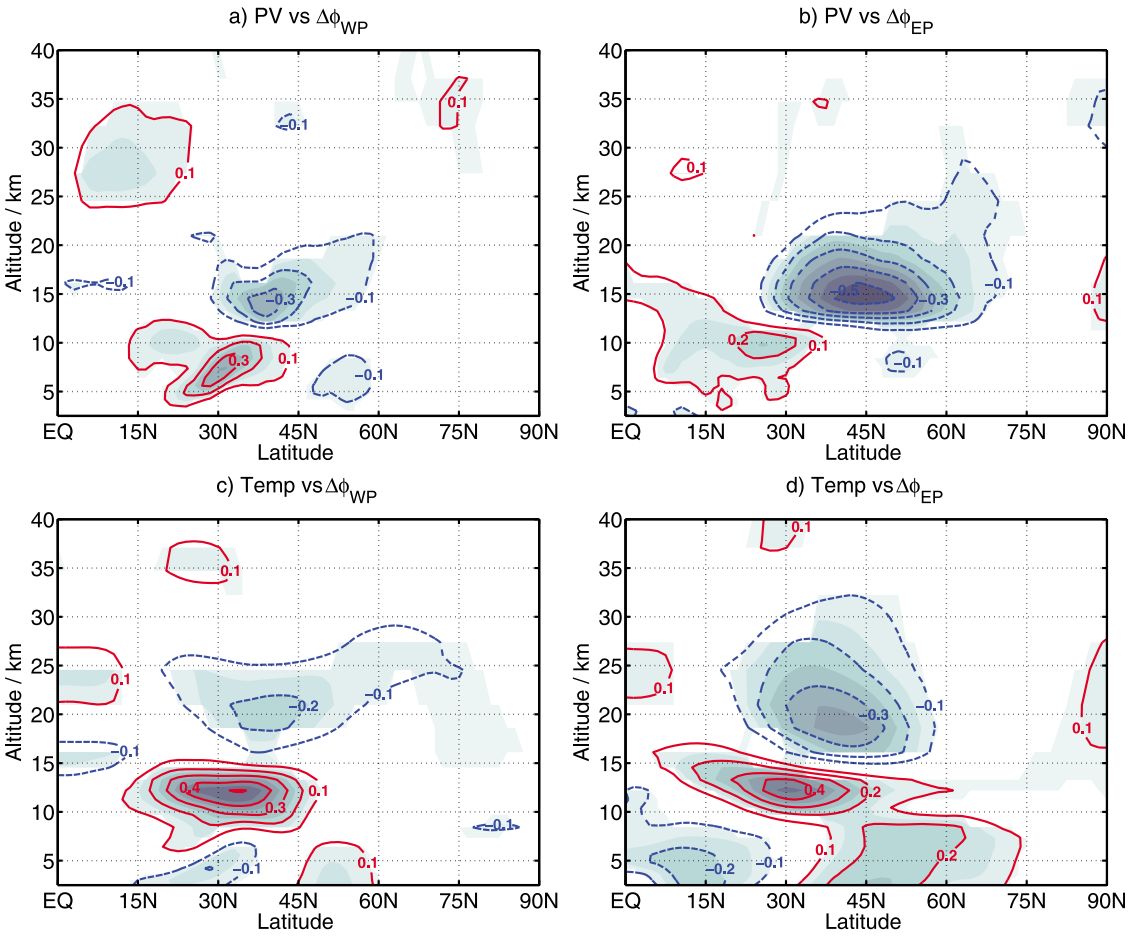

Figure 5. Latitude-altitude correlation profiles of the (a and b) PV and (c and d) potential temperature, θ, fields with $\overline{\Delta\phi}_{WP}$ (Figures 5a and 5c) and $\overline{\Delta\phi}_{EP}$ (Figures 5b and 5d). Contour intervals are 0.1, and the zero contour is not shown. Shaded plots represent correlations which are statistically significant at the 95% level (see the text for details).

[21] The characteristics of wave propagation may also be inferred from the Hovmöller diagrams in Figure 7. These diagrams are the composites of overlap width, $\overline{\Delta\phi}$, anomalies for events of large (> 1stdv) anomalies of $\overline{\Delta\phi}_{EP}$ and $\overline{\Delta\phi}_{WP}$ indices. We have identified the periods when the anomalies of $\overline{\Delta\phi}_{EP}$ (or $\overline{\Delta\phi}_{WP}$) were larger than one standard deviation, and defined the middle day of each period to be day zero. Only periods separated at least by 5 days were considered, giving a total of 92 and 104 events for the $\overline{\Delta\phi}_{EP}$ and $\overline{\Delta\phi}_{WP}$ indices, respectively. Then, for each longitude, λ, we computed the composite time series of $\Delta\phi(\lambda, t)$, with t running from day −20 to day 20. Structures of propagating wave patterns, with negative anomalies alternating with positive anomalies, are clearly evident in both Figures 7a and 7b. The dashed white lines in each panel represent a linear regression of the longitudes of maximum anomalies against the time lag. From the slopes of the lines, a propagation velocity of 25 ms^{-1} in the case of Figure 7a and 20 ms^{-1} in the case of Figure 7b, may be inferred. The velocities were estimated by considering the perimeter of a parallel at the mean latitude of the tropopausal break. The propagation velocities are much smaller than the mean zonal wind near the tropopausal break (see Figure 2), representing a westward propagation relative to the background flow, which is a characteristic of Rossby waves.

3.2. GPS Data

[22] The correlation patterns for the potential temperature, as shown in Figure 5, allow the comparison of the results from the ERA Interim reanalysis data with results obtained using GPS data. In order to perform such a comparison, the GPS profiles were grouped in the following manner. For each GPS profile at any NH latitude, all GPS profiles in the time interval ±2 hours, in the longitudinal band of ±2.5° and in the latitudinal band 25°–45°N were analyzed:

[23] (i) if no DT event was identified in the latitudinal band 25°–45°N, the reference profile was considered to be associated with single tropopause (ST) events in the subtropical NH;

[24] (ii) if at least two DT events were identified in the latitudinal band 25°–45°N, the reference profile was considered to be associated with DT events in the subtropical NH.

[25] For the foregoing specified longitudinal and time intervals, the mean number of GPS profiles in the latitudinal band 25°–45°N was less than 2, considering the cases when

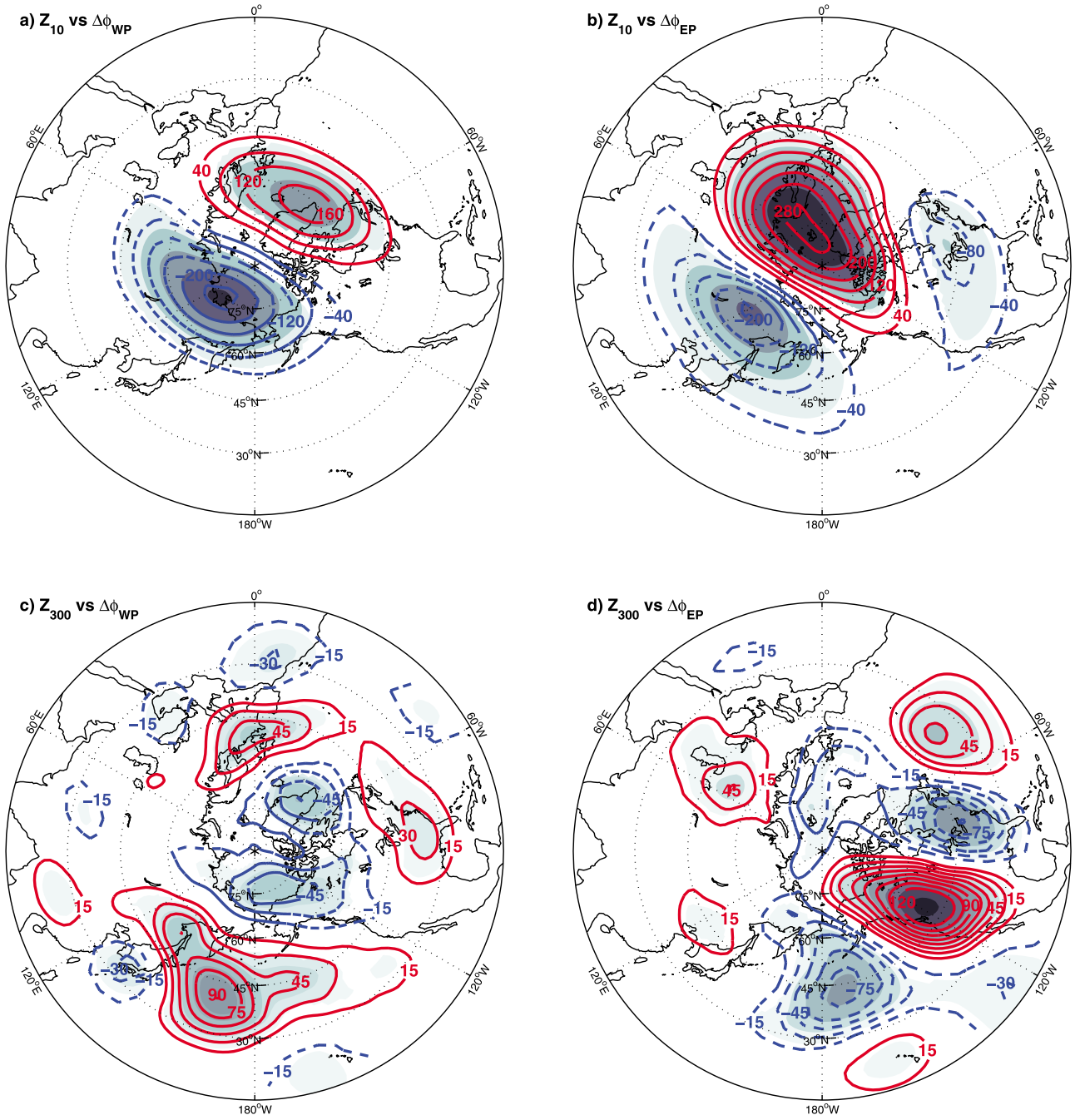

Figure 6. Same as Figure 4 but for the fields of (a and b) 10 and (c and d) 300 hPa geopotential height. Contour intervals are 40 gpm in Figures 6a and 6b and 15 gpm in Figures 6c and 6d.

at least one GPS profile was observed there. By attempting to use an appropriate sampling of the subtropical region, only those cases with at least two GPS profiles inside that region were retained in the analysis. For these cases, the mean latitudinal separation between the more equatorward and the more northward GPS profiles, inside the band 25°–45°N, was ~8°. Because of the requirement to have at least two GPS profiles in the subtropical region, only about 40% of the GPS profiles in that region were retained in the analysis. However, the results remained qualitatively the same when all cases with at least one GPS profile in the subtropical region were retained in the analysis.

[26] The identification of GPS profiles with DTs (STs) must be more likely when there is an increase (decrease) in the overlap of the tropical tropopause with the extratropical tropopause. Figure 8 shows the patterns of the differences between the mean potential temperatures of GPS profiles associated with DT and ST events (DT-ST) in the subtropical NH. Because of the zonal asymmetry in the DT frequency distribution shown in Figure 2 (the DT frequency

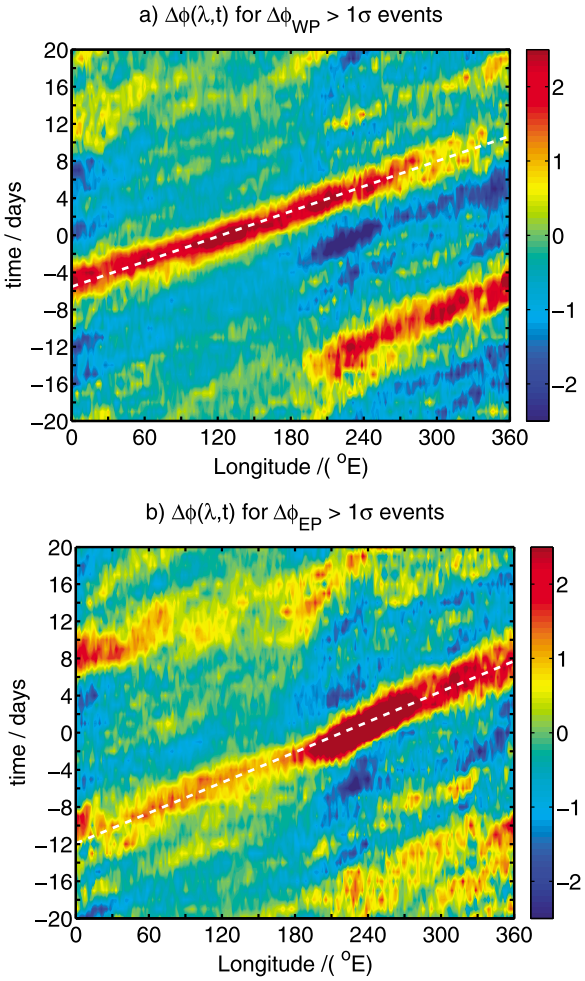

Figure 7. Hovmöller diagrams for the anomalies of the width of the tropopausal overlap. The diagrams are composites of 41-day time series where day zero is defined to be at the middle of periods of large (>1stdv) overlap anomalies in the (a) western Pacific ($\overline{\Delta\phi}_{WP}$) and (b) eastern Pacific ($\overline{\Delta\phi}_{EP}$). The units of the overlap are degrees of latitude.

distribution for the GPS data is similar), the difference patterns were calculated for two longitudinal sectors, namely sector 90–270°E where the DT events occur over a small range of latitudes and sector 90°W–90°E where the DT events occur over a broader range of latitudes. Here, we used much wider longitudinal sectors than those used in the definition of the $\overline{\Delta\phi}_{EP}$ and $\overline{\Delta\phi}_{WP}$ indices, in order to have a sufficient number of ST and DT events to obtain statistical significance. Moreover, the calculation of the composites for two different longitudinal sectors again shows that the characteristics associated with the variability of the overlap of the tropopauses are robust between the different regions. Because the amplitude of waves that propagate vertically must increase in proportion to the inverse of the square root of the mass density, the temperature differences, in the composites, were weighted by $\exp[-(z - z_0)/(2H)]$ with H = 7 km and z_0 = 13.5 km (the mean of the tropical and the extratropical tropopause positions). Both patterns of difference show baroclinic wave anomaly structures similar to the patterns of correlation seen in Figures 5c and 5d.

4. Concluding Remarks

[27] Assuming that the occurrence of DTs corresponds to an extension of the tropical tropopause over the extratropical one, we have argued that displacements of the tropopause that increase or decrease the meridional extension of the overlap must be associated with baroclinic wave anomalies of opposing sign in the subtropical UTLS. By regressing/correlating the PV, geopotential height or the potential temperature fields with measures of the meridional extension, $\overline{\Delta\phi}$, of the overlap, it was possible to reveal baroclinic

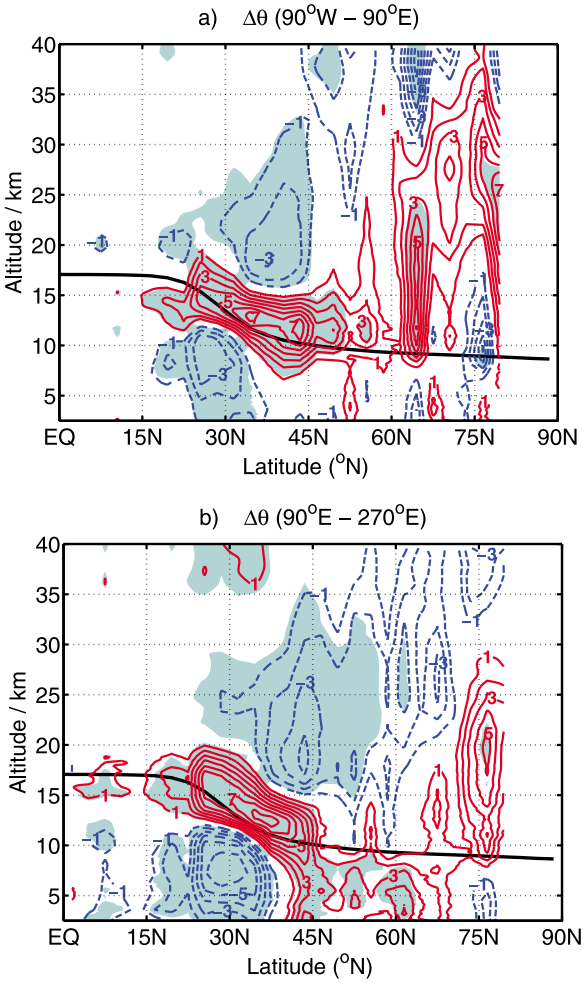

Figure 8. Potential temperature differences, $\Delta\theta$, between GPS profiles associated with DT and ST events in the subtropical latitude band 25°–45°N. Differences were calculated in sectors (a) 90°W–90°E and (b) 90°–270°E. The contour interval is 1 K and the zero contour is not shown. Shaded areas indicate statistically significant differences at the 99% level, using two-sided t-statistics. The thick black curve represents the mean height of the LRT1 by considering all GPS profiles. The temperature differences are plotted only if the numbers of ST and DT events are ≥50, with a meridional resolution of 3°.

wave anomaly structures. An additional test of the results obtained from the ERA Interim reanalysis data was provided by the analysis of high resolution temperature observations from the COSMIC GPS data. Moreover, the estimated propagation velocity of the anomalies in the meridional extension of the overlap indicates the rotational (Rossby) character of the waves.

[28] Finally, we contend that the analysis scheme presented herein may be useful for diagnostic studies of dynamics and transport in operational analysis (reanalysis) and in chemistry-climate model simulations. In such cases, the method must be extended in order to enable the identification of DTs associated with wave breaking, which causes the irreversible mixing of tropospheric tropical air with extratropical stratospheric air.

[29] **Acknowledgments.** This work was partially supported by the TRODIM Project (CGL2007-65891-C05-01) funded by the Spanish Ministry of Science and Innovation and by the DYNOZONE project (PTDC/CTE-ATM/105507/2008) funded by the FCT (Fundação para a Ciência e a Tecnologia, Portugal).

References

Añel, J. A., J. C. Antuña, L. de la Torre, J. M. Castanheira, and L. Gimeno (2008), Climatological features of global multiple tropopause events, *J. Geophys. Res.*, *113*, D00B08, doi:10.1029/2007JD009697.

Anthes, R. A., et al. (2008), The COSMIC/FORMOSAT-3 mission: Early results, *Bull. Am. Meteorol. Soc.*, *89*, 313–333, doi:10.1175/BAMS-89-3-313.

Birner, T. (2010), Recent widening of the tropical belt from global tropopause statistics: Sensitivities, *J. Geophys. Res.*, *115*, D23109, doi:10.1029/2010JD014664.

Castanheira, J. M., J. A. Añel, C. A. F. Marques, J. C. Antuña, M. L. R. Liberato, L. de la Torre, and L. Gimeno (2009), Increase of upper troposphere/lower stratosphere wave baroclinicity during the second half of the 20th century, *Atmos. Chem. Phys.*, *9*, 9143–9153, doi:10.5194/acp-9-9143-2009.

Dee, D. P., et al. (2011), The ERA-Interim reanalysis: configuration and performance of the data assimilation system, *Q. J. R. Meteorol. Soc.*, *137*, 553–597, doi:10.1002/qj.828.

Gettelman, A., et al. (2010), Multimodel assessment of the upper troposphere and lower stratosphere: Tropics and global trends, *J. Geophys. Res.*, *115*, D00M08, doi:10.1029/2009JD013638.

Pan, L. L., et al. (2009), Tropospheric intrusions associated with the secondary tropopause, *J. Geophys. Res.*, *114*, D10302, doi:10.1029/2008JD011374.

Randel, W. J., D. J. Seidel, and L. L. Pan (2007), Observational characteristics of double tropopauses, *J. Geophys. Res.*, *112*, D07309, doi:10.1029/2006JD007904.

Reichler, T., M. Dameris, and R. Sausen (2003), Determining the tropopause height from gridded data, *Geophys. Res. Lett.*, *30*(20), 2042, doi:10.1029/2003GL018240.

Santer, B. D., et al. (2003), Behavior of tropopause height and atmospheric temperature in models, reanalyses, and observations: Decadal changes, *J. Geophys. Res.*, *108*(D1), 4002, doi:10.1029/2002JD002258.

Schmidt, T., G. Beyerle, S. Heise, J. Wickert, and M. Rothacher (2006), A climatology of multiple tropopauses derived from GPS radio occultations with CHAMP and SAC-C, *Geophys. Res. Lett.*, *33*, L04808, doi:10.1029/2005GL024600.

Seidel, D. J., and W. J. Randel (2007), Recent widening of the tropical belt: Evidence from tropopause observations, *J. Geophys. Res.*, *112*, D20113, doi:10.1029/2007JD008861.

Vallis, G. K. (2007), *Atmospheric and Oceanic Fluid Dynamics: Fundamentals and Large-Scale Circulation*, 745 pp., Cambridge Univ. Press, Cambridge, U. K.

Wang, S., and L. M. Polvani (2011), Double tropopause formation in idealized baroclinic life cycles: The key role of an initial tropopause inversion layer, *J. Geophys. Res.*, *116*, D05108, doi:10.1029/2010JD015118.

J. M. Castanheira, Departamento de Física, CESAM, Universidade de Aveiro, Campus de Santiago, P-3810-193 Aveiro, Portugal. (jcast@ua.pt)

L. Gimeno, EPhysLab, Facultad de Ciencias de Ourense, Universidade de Vigo, Campus As Lagoas, E-32004 Ourense, España. (l.gimeno@uvigo.es)